optica

Integrated waveguide coupled Si_3N_4 resonators in the ultrahigh-Q regime

Daryl T. Spencer,[1,*] Jared F. Bauters,[2] Martijn J. R. Heck,[3] and John E. Bowers[1]

[1]Department of Electrical and Computer Engineering, University of California, Santa Barbara, California 93106, USA

[2]Aurrion, Inc., Goleta, California 93117, USA

[3]Department of Engineering, Aarhus University, Denmark

*Corresponding author: darylt@ece.ucsb.edu

Received 24 April 2014; revised 29 July 2014; accepted 3 August 2014 (Doc. ID 210465); published 8 September 2014

The vast majority of work on waveguide-coupled resonators focuses on decreasing losses in the waveguide and coupling region. Here we present fully integrated resonators based on an ultralow-loss Si_3N_4 waveguide platform. By tailoring the directional coupler excitation to the resonators, we are able to achieve lower loss single-mode coupling to multimode waveguide widths compared to straight bus waveguide directional couplers. This allows us to demonstrate record-high integrated waveguide coupled intrinsic quality factor (Q_{int}) values of 81 million at a 9.65 mm bend radius, with a future direction to both stronger and lower loss waveguide–resonator coupling. This result opens up integration possibilities for narrow linewidth integrated diode lasers, low noise feedback systems, microwave photonic research, and the ultrastable timing reference community.

OCIS codes: (140.4780) Optical resonators; (130.0130) Integrated optics; (230.7390) Waveguides, planar; (130.7408) Wavelength filtering devices.

http://dx.doi.org/10.1364/OPTICA.1.000153

The availability of fully integrable high-Q resonators, with quality factors approaching 100 million, can create a paradigm shift for the application of photonic integrated circuits (PICs) in a wide variety of applications. A monolithically integrated resonator and coupler allows for lithographic definition and control of the system, and integration with other optical devices that can greatly benefit from such narrowband filters and frequency references in the linear operation regime [1].

In the field of microwave photonics, these high-Q resonators can act as filters with a large tuning range over tens of gigahertz bandwidth. With bandpass widths of a few megahertz, such filters outperform best-in-class YIG-based microwave filters [2]. Such high-Q elements enable oscillators with lower-noise performance than oven-controlled crystal-based oscillators (OCXOs) in the microwave frequency range. Target applications include 60 GHz wireless systems where these oscillators can increase the spectral efficiency over systems based on CMOS technology, by enabling complex modulation formats, or increase the link distance by improving the signal-to-noise ratio [3]. This added energy efficiency is essential for ubiquitous implementation of future 4G and 5G wireless systems. In coherent Doppler radars, e.g., automotive, the probability of detection of, especially, small and slow-moving targets will be increased. This increase in probability can be up to 40% for 5 dB decrease in noise [4]. In the optical domain, such oscillators can be used to create combs of optical frequencies, with very accurate spacings. These combs can act as optical "rulers" for precision spectroscopy in fields such as high-resolution metrology and gas sensing, with applications to lidar and satellite positioning systems [5]. PIC-based gyroscopes based on such high-Q resonators will outperform MEMS-based gyros and become competitive with fiber-optic and ring-laser-based approaches for tactical grade gyro applications requiring resolutions of 0.1°/h [6,7].

Generally, waveguide platforms have achieved low loss using Si [8], InP [6], doped silica [9,10], or Si_3N_4 [11–16]. In Fig. 1, we show the state of the art in resonator performance for integrable coupling schemes, typically horizontal or vertical evanescent waveguide coupling. The trade-off between quality factor and bend radius is shown in both the microring regime (20–200 μm radius) and large bend radius regime (1–10 mm radius). Recent Si_3N_4 results from our group are highlighted in the 1–10 mm bend radius range, with new results in this Letter showing the highest integrated Q_{int} ever reported, to our knowledge.

2334-2536/14/030153-05$15/0$15.00

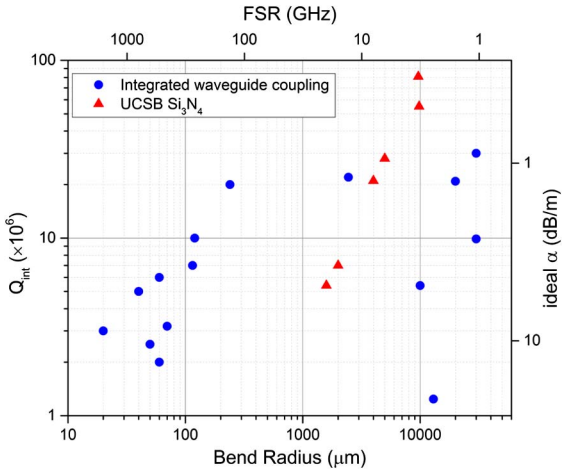

Fig. 1. State-of-the-art resonator comparison of Q_{int} versus bend radius for integrated waveguide-coupled resonators [6,8–16]. The propagation loss (α) and FSR are scaled assuming $\lambda = 1550$ nm, $n_{eff} = n_g = 1.5$, and lossless directional couplers according to Eq. (1). UCSB Si_3N_4 results [15,16], including this Letter, are highlighted in red triangles.

The theoretically obtainable Q_{int} for a given system takes into account the waveguide propagation loss, α (dB/m), directional coupler power ratio, κ, and excess directional coupler power loss per pass, γ. Equation (1) shows the obtainable Q_{load} for a given propagation loss [17]:

$$Q_{load} = \frac{2\pi n_{eff} L}{\lambda}[\kappa + \alpha L + \gamma]^{-1}. \quad \textbf{(1)}$$

The excess coupler loss adds parasitic loss and becomes important as it approaches the round-trip propagation loss αL. Parasitic losses can occur from scattering loss in the coupler as well as coupling into unwanted higher order or radiation modes as the coupling gap decreases, which occur for even high bend radius devices [18].

Figure 2 plots Eq. (1) without the power coupling term, κ, which is usually extracted through data analysis. In the low-loss regime of 0.2 dB/m and at a bend radius of 10 mm, efficient directional couplers with less than −30 dB excess insertion loss are required to not add appreciable loss to the system. Such low

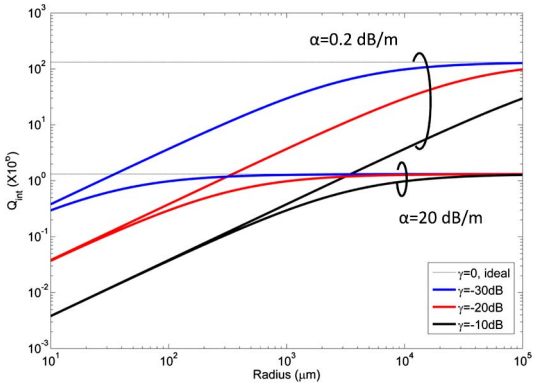

Fig. 2. Theoretically obtainable Q_{int} for a given directional coupler excess loss value, γ, and propagation loss, α, according to Eq. (1).

insertion losses are not possible to simulate in commercial software packages, and in this Letter we present experimental results showing low-loss adiabatic directional couplers in 81 million Q_{int} resonators. In our work, we target low confinement, fully monolithic Si_3N_4 waveguide structures that will be useful for future integration with silicon [19,20] and hybrid silicon III–V components [21]. High-quality Si_3N_4 is deposited via low pressure chemical vapor deposition (LPCVD) on a 15-μm-thick thermally grown SiO_2 layer on a silicon substrate. For this work, a thin 40 nm film is chosen to lower the confinement factor and decrease sidewall scattering loss at the expense of a higher bend radius device. Contact lithography defines the ring resonators and directional couplers. The bus waveguide-to-ring gap is generally >1 μm wide due to the low waveguide confinement and low coupling needed for high-Q resonators. The gaps in this study were chosen based on previous experimental results, and are identical on the add and drop ports. 3.1 μm of SiO_2 is deposited via LPCVD in three layers, with an 1150°C anneal after each layer. The sample is then chemically mechanically polished and a 15 μm thick thermal SiO_2 on Si top cladding is wafer bonded after plasma activation of the surfaces. The samples are annealed at 950°C for 3 h and diced for testing. The completed cross section is shown in Fig. 3(a), and further fabrication details can be found in [15,22].

The waveguide width now defines the number of supported modes. 7-μm-wide waveguides have produced single-mode resonators with 55 million Q_{int} [15]. Based on our previous work on ultralow-loss delay lines, the lowest loss of (0.045 ± 0.04 dB/m) has been observed in multimode waveguide spirals [22]. Assuming directional couplers without excess loss, this mean propagation loss in a resonator corresponds to a Q_{int} of 575 million. This low-loss core geometry of 11 μm × 40 nm has now been implemented in add–drop ring resonators at a bending radius of 9.65 mm, consistent with a free spectral range (FSR) of 3.3 GHz near 1580 nm. Figures 3(b)–3(d) present the simulated mode profiles for the three supported modes, TE_0, TM_0, and TE_1. The low-loss mode of interest is the TE_0 mode, which has an effective area of 33 μm^2 and core confinement factor of 3% at 1580 nm.

To study multimode resonators, care must be taken in the directional coupler design. In addition to requiring low excess coupler loss, as discussed earlier, any unwanted coupling to higher order modes will produce multiple families of resonances with different FSRs, and effectively lower the resonator Q. These corrupted spectra will produce spurious tones when filtering noise for applications such as microwave photonics. Figure 4 outlines directional coupler layouts for waveguide

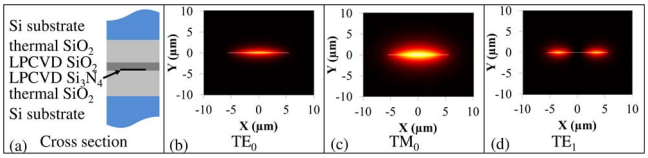

Fig. 3. (a) Waveguide cross section and (b)–(d) all supported modes of the 11 μm × 40 nm Si_3N_4 core geometry at a 9.65 mm bending radius, simulated with FIMMWAVE.

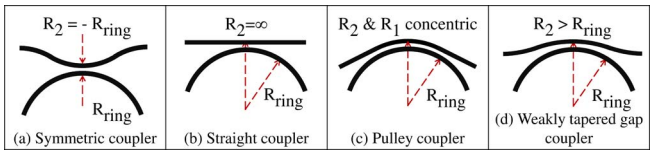

Fig. 4. Directional coupler layouts for ring resonators. The tapering of the gap is strongest for (a) symmetric coupling and identical for the (b) straight and (c) pulley couplers, while the (d) weakly tapered gap coupler smoothes the gap transition. We fabricated straight and weakly tapered gap couplers in this study.

coupled ring resonators. Figure 4(a) is a traditional symmetric coupler that is exactly beta matched but has the strongest tapering into the coupling region. Figures 4(b) and 4(d) show the two directional coupler designs studied in this Letter. The first was a straight bus waveguide coupled to the ring resonator, or "straight" coupler. We have studied these couplers on higher contrast waveguides, and our splits show an excess loss associated with a decrease in gap, yielding inefficiencies that limit the quality factor [15]. Additionally, these couplers had appreciable coupling to higher order modes, producing corrupted resonator spectra. To overcome this, we have designed a second "weakly tapered gap" directional coupler [Fig. 4(d)]. As a first experiment, we fabricate the bus waveguide with a bend radius that is 30% larger than the resonator radius to have two effects. The first is to decrease the beta mismatch between two arms of the coupler such that more efficient excitation of the fundamental mode is achieved over higher order modes. Additionally, weakly tapering the gap will yield a more adiabatic transition region from the input bus waveguide to the coupling region than the pulley, symmetric, and straight couplers of Figs. 4(a)–4(c), which we hypothesize will lower the excess loss of the coupler.

Figure 5 shows the simulated n_{eff} and n_g of the waveguide geometry's two TE modes, taking into account waveguide and bulk material chromatic dispersion [23,24]. We are mainly interested in the low-loss TE_0 mode. However, excitation of higher order modes from input tapers and/or directional couplers can corrupt the spectrum through multiple families

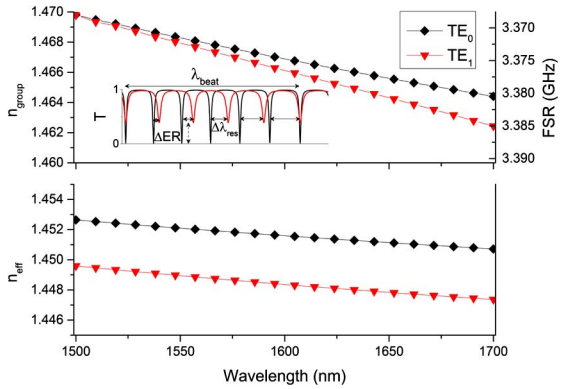

Fig. 5. Simulated TE effective and group indices for the 11 μm × 40 nm Si_3N_4 multimode waveguides studied in this Letter. Due to the fundamental TE_0 mode having a higher group index, there will be a relative resonance wavelength separation, $\Delta\lambda_{\text{res}}$ and overall beat wavelength, λ_{beat} (inset).

of resonance peaks that would have a difference of only 3 MHz in FSR at 1580 nm. This Vernier effect is shown schematically in Fig. 5 (inset) where the high n_g mode (TE_0) contains one extra resonance across a large wavelength span, termed the beat wavelength, λ_{beat}. The relative extinction ratio (ΔER) is referenced to the high n_g TE_0 mode. The separation between adjacent resonances of the two transverse modes, $\Delta\lambda_{\text{res}}$, increases with wavelength in reference to the high n_g mode. The TE_0 mode will thus have $m+1$ FSRs in λ_{beat}, where m is the number of TE_1 FSRs. The ratio of group indices is then

$$\frac{n_{g\text{TE}_0}}{n_{g\text{TE}_1}} = 1 + \frac{1}{m}. \tag{2}$$

Since the number of FSRs in λ_{beat} is dependent only on the group index ratio, measuring resonators with long cavity lengths allows for the beat wavelength to be within a reasonable measurable range. For a typical wavelength sweep of 100 nm, a 9.65 mm radius resonator will have ~3500 FSRs and a resolution down to 0.03% change in group index ratio. A higher n_g ratio will produce multiple beat frequencies in this range. To achieve the same measurement resolution would require a setup with high thermal and mechanical stability, and kilohertz level sweep accuracy for FSR extraction, such as a RF domain measurement [25,26]. We will experimentally analyze this multimode situation in the following section and use the beat wavelength to extract the resonances of each mode.

Measurement of the add–drop high-Q resonators was done in the frequency domain using a tunable external cavity laser (Agilent 86142A). The slowest sweep speed of 0.5 nm/s was used so as to avoid any ring-down effects that could occur [27]. Cleaved SMF28 fiber was used for coupling in/out of the device, and the output was coupled to a high-responsivity InGaAs detector. The photocurrent was terminated on a 1 GHz oscilloscope to enable high data rate acquisition. The wavelength regime of 1580 nm was studied for the highest Q factors, as this yields the lowest propagation loss of the platform [22]. A polarization controller was also used on the input to excite the lower loss TE polarization. The TM polarization, which has a lower confinement and higher bend loss than the TE_0 mode, was not excited due to the polarizing nature of S bends on the Si_3N_4 platform [28]. All results are averaged over multiple closely spaced resonances within 0.5 nm.

We first analyze the relative resonant wavelengths and extinction ratios (ERs) of the two directional coupler designs in the L band. Figure 6 compares a 5 μm gap straight coupler with a 3.8 μm weakly tapered gap coupler. The beat wavelength, λ_{beat}, is extracted from the two overlap points by curve fitting a second-order polynomial that accounts for dispersion. With the same nominal path length, the two resonators show $\lambda_{\text{beat}} = (73 \pm 2)$ nm, corresponding to ≈2500 resonances across this range. The ratio of n_g between TE_0 and TE_1 is found to be 1.00039 ± 0.00002, which matches well with our simulated ratio of 1.00040 ± 0.00002, for an n_g of 1.4674 and 1.4668, respectively, in the region of interest.

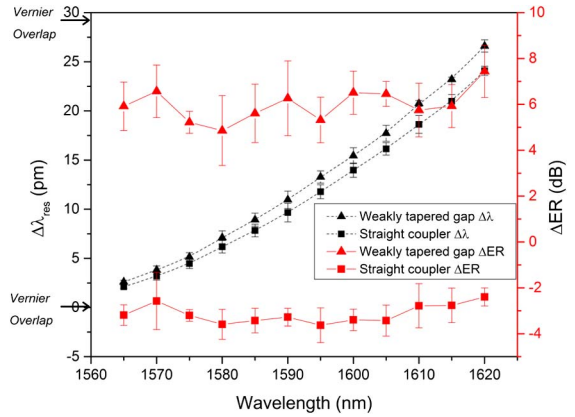

Fig. 6. Relative resonance wavelengths and ERs for the TE_0 and TE_1 modes across the region of interest. All numbers are taken relative to the fundamental TE_0 mode and averaged over multiple closely spaced resonances every 5 nm. The weakly tapered gap directional coupler resonator shows a beat wavelength of 73 nm similar to that of a straight directional coupler resonator, with an increase in absolute and relative ER.

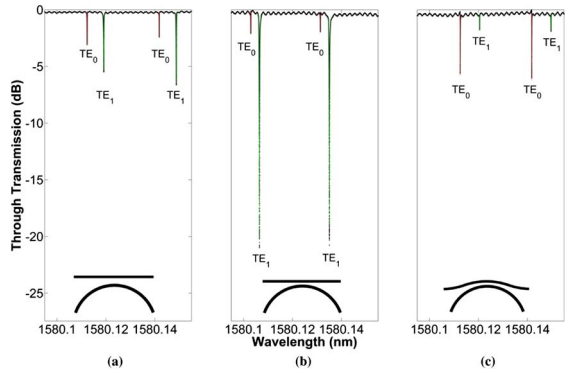

Fig. 7. Resonator spectra and fits near 1580 nm for three different directional coupler designs: (a) 5 μm straight bus waveguide, (b) 3.8 μm straight bus waveguide, and (c) 3.8 μm weakly tapered gap waveguide.

Additionally, the ΔER between modes in the two directional coupler designs changes sign. Due to these observations, we conclude that we have achieved stronger coupling to the fundamental TE_0 mode with the weakly tapered gap directional coupler as compared to the straight directional coupler.

Next, we analyze the individual resonances near 1580 nm to extract Q_{int} values. First, we show a comparison of straight couplers with two different waveguide–resonator bus gaps, 3.8 and 5 μm, in Figs. 7(a) and 7(b), respectively. The modes are labeled according to the previous modal analysis, and all devices are undercoupled due to the identical coupler layouts on the add and drop ports. For both straight coupler gaps, the higher order TE_1 mode is coupled much stronger than the lower loss fundamental mode, as observed by the magnitude of the ER. In this regime, the TE_0 mode has a maximum Q_{int} factor of 63 million at a 5 μm gap, similar to the results of the previous generation [15]. However, using a weakly tapered gap directional coupler at a 3.8 μm minimum gap at bus radius of 12.545 mm, we couple stronger and more efficiently to the fundamental TE_0 mode. This has the consequence of a higher ER than for the TE_1 mode, as seen in Fig. 7(c), as well as an even higher Q_{int} factor of 81 million, outlined in Table 1. This is the largest Q_{int} factor for a monolithic waveguide coupled resonator system to date, to our knowledge.

We have presented results on the highest integrated resonator Q_{int} values to date, to our knowledge, with a value of 81 million at a 9.65 mm bend radius. Using low confinement Si_3N_4/SiO_2 waveguides, we have utilized multimode waveguide widths and spectral analysis to extract propagation losses and directional coupler information for weakly tapered coupling gaps. These weakly tapered gap directional couplers are a critical path forward to higher quality factor integrated resonators that require increasingly efficient and low-loss coupling. Improved design of beta matched weakly tapered gap couplers should help reduce the loss of directional couplers, and full utilization of the Si_3N_4 platform, with record propagation loss of 0.05 dB/m, should be able to yield resonators with Q_{int} values of 600 million.

FUNDING INFORMATION

Defense Advanced Research Projects Agency (DARPA) (HR0011-12-C-0006); National Science Foundation (NSF) (DGE-1144085)

ACKNOWLEDGMENTS

The authors would like to thank Josh Conway, Scott Rodgers, Dan Blumenthal, Arne Leinse, and René Heideman for helpful discussions. The devices were partially fabricated at LioniX BV.

Table 1. Measured and Extracted Resonator Parameters for the Three Directional Coupler Designs Studied at 1580 nm, Assuming No Parasitic Losses ($\gamma = 0$)[a]

Gap (μm)	Mode	Q_{int} ($\times 10^6$)	Q_{load} ($\times 10^6$)	RTL (dB)	α (dB/m)	κ (%)	ER (dB)
5.0	TE_0	63	46	0.026	0.42	0.11	2.7
5.0	TE_1	27	13	0.061	1.00	0.72	6.1
3.8	TE_0	35	28	0.047	0.78	0.13	1.8
3.8	TE_1	41	4	0.038	0.63	4.07	20.2
3.8-taper	TE_0	**81**	**42**	**0.019**	**0.32**	**0.20**	**5.6**
3.8-taper	TE_1	30	26	0.055	0.90	0.11	1.4

[a]The bend radius is 9.65 mm, and nominal gap widths are shown. The measured Q_{load} and ER allow extraction of the power coupling coefficient (κ), Q_{int}, propagation loss (α), and round-trip loss (RTL). The RTL is the upper bound on γ for two directional couplers.

REFERENCES

1. M. J. R. Heck, J. F. Bauters, M. L. Davenport, D. T. Spencer, and J. E. Bowers, "Ultra-low loss waveguide platform and its integration with silicon photonics," Laser Photon. Rev., doi: 10.1002/lpor.201300183 (posted online March 5, 2014).
2. D. Marpaung, C. Roeloffzen, R. Heideman, A. Leinse, S. Sales, and J. Capmany, Laser Photon. Rev. **7**, 506 (2013).
3. D. Cabric, M. S. W. Chen, D. A. Sobel, S. Wang, J. Yang, and R. W. Brodersen, EURASIP J. Wirel. Commun. Netw. **2006**, 1 (2006).
4. J. R. Vig, "Introduction to quartz frequency standards," Res. Dev. Tech. Rep. SLCET-TR-92-1 1 (U.S. Army Electronics Technology and Devices Laboratory, 1992).
5. P. Maddaloni, M. Bellini, and P. De Natale, *Laser-Based Measurements for Time and Frequency Domain Applications* (Taylor & Francis, 2013).
6. C. Ciminelli, F. Dell'Olio, M. N. Armenise, F. M. Soares, and W. Passenberg, Opt. Express **21**, 556 (2013).
7. C. Ciminelli, F. Dell'Olio, and M. N. Armenise, IEEE Photon. J. **4**, 1844 (2012).
8. A. Biberman, M. J. Shaw, E. Timurdogan, J. B. Wright, and M. R. Watts, Opt. Lett. **37**, 4236 (2012).
9. R. Adar, Y. Shani, and C. Henry, Appl. Phys. Lett. **58**, 444 (1991).
10. R. Adar, M. R. Serbin, and V. Mizrahi, J. Lightwave Technol. **12**, 1369 (1994).
11. Q. Li, A. A. Eftekhar, M. Sodagar, Z. Xia, A. H. Atabaki, and A. Adibi, Opt. Express **21**, 18236 (2013).
12. A. Gondarenko, J. S. Levy, and M. Lipson, Opt. Express **17**, 11366 (2009).
13. K. Luke, A. Dutt, C. B. Poitras, and M. Lipson, Opt. Express **21**, 22829 (2013).
14. L. Zhuang, D. Marpaung, M. Burla, W. Beeker, A. Leinse, and C. Roeloffzen, Opt. Express **19**, 23162 (2011).
15. D. T. Spencer, Y. Tang, J. F. Bauters, M. J. R. Heck, and J. E. Bowers, in *IEEE Photonics Conference* (Institute of Electrical and Electronics Engineers, 2012), pp. 141–142.
16. M.-C. Tien, J. F. Bauters, M. J. R. Heck, D. T. Spencer, D. J. Blumenthal, and J. E. Bowers, Opt. Express **19**, 13551 (2011).
17. O. Schwelb, J. Lightwave Technol. **22**, 1380 (2004).
18. D. Ding, M. J. A. de Dood, J. F. Bauters, M. J. R. Heck, J. E. Bowers, and D. Bouwmeester, Opt. Express **22**, 6778 (2014).
19. T. Tsuchizawa and K. Yamada, IEEE J. Sel. Top. Quantum Electron. **17**, 516 (2011).
20. J. F. Bauters, M. L. Davenport, M. J. R. Heck, J. K. Doylend, A. Chen, A. W. Fang, and J. E. Bowers, Opt. Express **21**, 544 (2013).
21. M. Piels, J. Bauters, M. Davenport, M. Heck, and J. Bowers, J. Lightwave Technol. **32**, 817 (2013).
22. J. F. Bauters, M. J. R. Heck, D. D. John, J. S. Barton, C. M. Bruinink, A. Leinse, R. G. Heideman, D. J. Blumenthal, and J. E. Bowers, Opt. Express **19**, 24090 (2011).
23. H. R. Philipp, J. Electrochem. Soc. **120**, 295 (1973).
24. T. Bååk, Appl. Opt. **21**, 1069 (1982).
25. N. Uehara and K. Ueda, Appl. Phys. B **61**, 9 (1995).
26. B. J. J. Slagmolen, M. B. Gray, K. G. Baigent, and D. E. McClelland, Appl. Opt. **39**, 3638 (2000).
27. A. A. Savchenkov, A. B. Matsko, V. S. Ilchenko, and L. Maleki, Opt. Express **15**, 6768 (2007).
28. J. F. Bauters, M. J. R. Heck, D. Dai, J. S. Barton, D. J. Blumenthal, and J. E. Bowers, IEEE Photon. J. **5**, 6600207 (2013).